CHALMERS

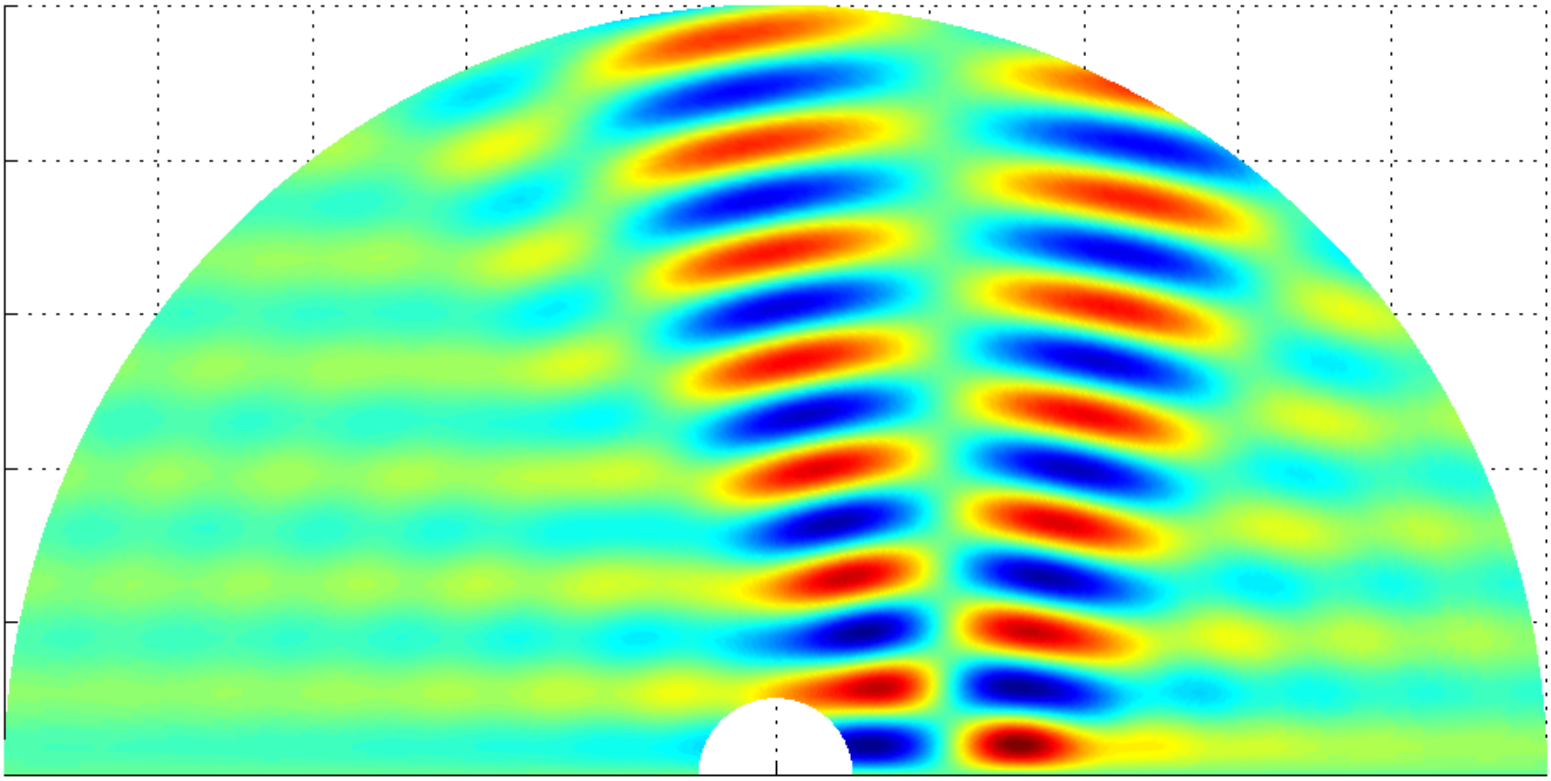

Modeling of ultrasonic nondestructive testing of pipes

Master's Thesis in Applied Mechanics

JACOB RUBENSON

Department of Applied Mechanics
Chalmers University of Technology
Gothenburg, Sweden 2011
Master's Thesis 2011:1

MASTER THESIS IN SOLID AND STRUCTURAL MECHANICS

Modeling of ultrasonic nondestructive testing of pipes

Jacob Rubenson

Department of Applied Mechanics
Division of Dynamics
CHALMERS UNIVERSITY OF TECHNOLOGY
Göteborg, Sweden 2011

Modeling of ultrasonic nondestructive testing of pipes

Jacob Rubenson

Master's thesis in Solid and Structural Mechanics 2011:58
ISSN 1652-8557
Department of Applied Mechanics
Division of Dynamics
Chalmers University of Technology
SE-412 96 Göteborg
Sweden

Chalmers Reproservice
Göteborg, Sweden 2011

Abstract

Nondestructive testing is a method used for investigating the presence of cracks in a medium. The testing method does not require removing nor damaging the medium. Nondestructive testing is often used in different industrial applications where there are large object which may contain toxic contents, e.g. in nuclear power plants.

The department of Applied Mechanics is developing a model for elastodynamic scattering of a crack in a pipe. This thesis work is a first step in developing this model. In this thesis work only anti-plane motion for a fixed frequency is considered, i.e. SH waves. The limitations are on the problem definition, not on the method of derivation. The generality of the methods makes it possible to continue working expanding the model with a more general problem definition.

The result is presented as three dimensional contour graphs for the displacement field. It is visible that the curvature of the pipe influences the results. Since there is experimental data to compare with it is hard to determine the accuracy of the results. Hope fully a continuation of this thesis work can verify the result with experimental data.

Acknowledgements

I'd like to thank:

Anders Boström, my supervisor who has guided my through this project with fruitful discussions.

Peter Folkow, for answering many questions and for introducing elastic wave motion in the course *Fudamental structural Dynamics* which I enjoyed greatly.

All the nice people working at the department of Applied Mechanics for making the working at your office easy.

My family, who supported me through my time at Chalmers.

Jacob Rubenson, Gothenburg November 14, 2011

Foreword

I applied for this Master's thesis project mainly because of the usage of analytical methods. The first years at Engineering Physics introduced me to several analytical methods however often to problems without many geometrical constraints. In this thesis work I learned how to use analytical tools for more complicated problems, in contrast to the numerical methods which were extensively during the Master's Programme.

Contents

1

Introduction

Nondestructive testing of pipes, what does it mean and what usage is there for it? Nondestructive testing is performed on pipes while they are still connected as long as the properties of the pipes are known. The fact that the pipe does not need to be removed ensures that the content of the pipe is intact at all time while testing. These properties are beneficial if the content is hazardous or if the pipe is hard to remove.

In Sweden one of the applications of nondestructive testing is at the nuclear power plants. The pipes are large and it would lead to a disaster if any of the toxic contents would leak into the environment. Chalmers department of Applied Mechanics has a history of working with nondestructive testing with the Swedish Radiation Safety Authority*. The department of Applied Mechanics has taught several Ph.D.'s in the area nondestructive testing.

The cracks are found by transmitting ultrasonic waves into the pipe. To determine what type of crack that is present, if any, the reflection is analyzed and compared to developed models. The ultrasonic waves are created using a piezoelectric probe and the receiver is a similar device.

The development of new and more realistic mathematical models are crucial not only for detecting cracks but also for understanding. To both understand and describe mathematically the nature of elastodynamic scattering is both an important and a challenging task. It is a priority for universities to further their understanding of their field of expertise. The reputation of the university is to some extent dependent on the quality of the research. This is a reason for performing good research at a university, also universities with good reputations receives larger monetary grants.

*SSM: Strålskyddsmyndigheten

Until this thesis the work at with nondestructive evaluation, at Chalmers, is using the approximation that the pipe is locally flat, i.e. that the curvature of the pipe is small. This thesis aims to investigate the how a radial crack in the $r\varphi$-plane of a pipe scatters an incoming wave. The department of Applied Mechanics plans to model an arbitrarily aligned crack in pipe and solving the scattered field in the future. This thesis is small step to begin the work for the full pipe.

1.1 Layout of the thesis

The layout of this thesis will be in four parts; one part introducing the subject and some key definitions, one part covering the analytical derivations, one part presenting the result and one part discussing it.

1.2 Problem definition

This thesis considers the propagation of waves inside a cylindrical pipe. This is to determine both the incident field and the field scattered from the crack. Mathematically it is stated as solving the elastodynamic equations of motion in a cylindrical geometry for two different cases; with a crack and without a crack present.

The boundary conditions for the incident field is that there is a known stress propagates in the radial direction on a limited part of the outer boundary and stress free on the rest of both the inner and outer diameter. The boundary conditions for the crack is a bit more complicated and are discussed further in section 2.4.

There are many different methods of solving these kinds of problems; eigenfunction expansion, Finite Element Method, Boundary Element Method or using Green's functions. The method used in this thesis uses both eigenfunction expansion and Green's function method.

1.3 Limitations of the thesis

The limits of this thesis is to only consider a time harmonic problems and an anti-plane motion in the $r\varphi$-plane. These approximations ensure that a scalar uncoupled partial differential equation is obtained instead of a vector one. The method used for the calculations is called the hypersingular integral method. Regularization is performed using Chebyshev functions. This method reduces the problem to a multiple integral which is evaluated numerically. This method can solve problems in different geometries both in 2D and 3D [1].

1.4 Definitions

1.4.1 Green's Function

Green's functions are a type of functions which are used for solving differential equations [2]. They are by definition continuous whilst their derivative is not [2]. Generally the Green's function is defined together with a linear operator where the differential equation (DE) is defined. To obtain the Green's function the is differential equation solved with a point source as the inhomogeneous part. This is explained in more detail in section 2.2.

1.4.2 Hypersingular integral

Hypersingular integrals which have a singularity

$$\int_a^b \frac{F(t)}{(t-x)^n} \mathrm{d}t, \quad x \in]a,b[, \tag{1.1}$$

where $n = 2$ [3], These types of integrals are not integrable in a ordinary way [3] and in this thesis the integral is regularized using Chebyshev functions, which are defined in appendix 5.2.

1.4.3 Abbreviations and symbols

The following abbreviations and symbols are used in this master thesis are shown in table 1.1 and 1.2 respectively.

Table 1.1: The abbreviations used

GFM	Green's functions method
FEM	Finite element method
BEM	Boundary element method
PDE	Partial differential equation
DE	Differential equation

Table 1.2: The symbols used

$\mathbf{x}$	Vector
$\hat{\mathbf{x}}$	Unit vector
Δ	Laplace operator
∇^2	Vector Laplace operator
∂_φ	derivative w.r.t. φ
$\overline{z}$	Complex conjugate
$\mathrm{J}_m(x)$	Bessel function of order m
$\mathrm{N}_m(x)$	Neumann function of order m
$\mathrm{H}_m^{(1)}(x)$	Hankel function of the first kind order m
$\psi_m(x)$	Chebyshev function of order m
$\dot{u}$	Derivative w.r.t time

2

Mathematical models

This chapter contains all of the necessary derivations in order to calculate the incident and the scattered fields. The techniques introduced here are described more generally to later be applied to the specifics of this thesis. First the basics of elastodynamics is introduced and afterwards the solutions for incident and scattered fields are derived.

2.1 Elastodynamics

The elastodynamic equation of motion was first introduced in the course *Fundamental Structural Dynamics*,

$$\begin{aligned} c_p^2 \nabla(\nabla \cdot \mathbf{u}) - c_s^2 \nabla \times (\nabla \times \mathbf{u}) - \ddot{\mathbf{u}} = 0, \\ c_p = \sqrt{\frac{\lambda + 2\mu}{\rho}}, \\ c_s = \sqrt{\frac{\mu}{\lambda}}. \end{aligned} \tag{2.1}$$

λ, μ are identified as Lamé constants and together with the density ρ they define the different wave propagation speeds c_p and c_s. For the derivation of elastodynamic equation of motion c.f. Boström [4] or Graff [5]. As stated in the limitations only time harmonic solutions are considered in this thesis. This simplifies the elastodynamic equation to

$$\begin{aligned} \Big(k_p^{-2} \nabla(\nabla \cdot \mathbf{u}) - k_s^{-2} \nabla \times (\nabla \times \mathbf{u}) + \mathbf{u}\Big) \exp(-i\omega t) = 0, \\ k_p = \omega \sqrt{\frac{\rho}{\lambda + 2\mu}}, \\ k_s = \omega \sqrt{\frac{\rho}{\mu}}. \end{aligned} \tag{2.2}$$

The factor $\exp(-i\omega t)$ is omitted for the rest of this thesis. It is recognized that the propagation speeds have been replaced by wavenumbers (k_p, k_s).

Two things are shown in the introduction to elstodynamics; firstly that the elastodynamic equation of motion consists of one pressure and two shear components, secondly it is shown that for the vector equation, equation (2.2), becomes a scalar equation for anti-plane motion in 2D.

2.1.1 Decomposition of the displacement field

To show that the displacement field consists of a pressure and two shear components the Helmholtz decomposition [4] is used,

$$\mathbf{u} = \nabla\Psi + \nabla \times \mathbf{\Phi}. \tag{2.3}$$

Inserting the Helmholtz decomposition into the equation of motion, assuming $\nabla \cdot \mathbf{\Phi} = 0$ as well as using some vector identities one receives two decoupled equations

$$\Delta\Psi + k_p^2\Psi = 0, \tag{2.4}$$

$$\nabla^2\mathbf{\Phi} + k_s^2\mathbf{\Phi} = 0. \tag{2.5}$$

The scalar equation can be solved in this form, however, the vector equation can be decomposed further into

$$\mathbf{\Phi} = \mathbf{n}\phi_1 + k_s^{-1}\nabla \times \mathbf{n}\phi_2 \tag{2.6}$$

where k_s is the wavenumber and $\mathbf{n}$ is a constant vector. Both ϕ_1 and ϕ_2 are solutions to

$$\Delta\phi_i + k_s^2\phi_i = 0, \quad i = 1,2. \tag{2.7}$$

Inserting (2.6) into (2.3) the following is obtained

$$\mathbf{u} = \nabla\Psi + \nabla \times (\mathbf{n}\phi_1) + \nabla \times (k_s^{-1}\nabla \times (\mathbf{n}\phi_2)) \equiv \mathbf{u}_P + \mathbf{u}_{SV} + \mathbf{u}_{SH} \tag{2.8}$$

it is clearly seen that there are three components to the displacement field; a pressure/primary part and two shear/secondary parts.

The vector $\mathbf{n}$ is often chosen such that it is parallel to a surface normal for the problem at hand. Calling the shear waves in-plane and anti-plane waves is a historical notation from the 2D case. Often $\mathbf{n}$ is chosen as it is parallel to the normal vector of the surface where the boundary condition is applied. If the vector is chosen wisely the notion of in-plane and anti-plane motion is evident.

2.1.2 Reduction to a scalar equation

To show that the coupled vector PDE reduces to a decoupled scalar PDE, the vector $\mathbf{n} = \hat{\mathbf{z}}$ is chosen, then equation (2.8) reduces to

$$\begin{aligned}\mathbf{u} = \hat{\mathbf{r}}(\partial_r\Psi + r^{-1}\partial_\varphi\phi_1 - A\partial_{rz}\phi_2) + \hat{\boldsymbol{\varphi}}(r^{-1}\partial_\varphi\Psi - \partial_r\phi_1 + Ar^{-1}\partial_{rz}\phi_2) + \\ + \hat{\mathbf{z}}(Ar^{-2}\partial_{\varphi\varphi}\phi_2 - A\partial_{rr}\phi_2).\end{aligned} \tag{2.9}$$

Assuming that the motion is 2D, in this case $\mathbf{u} = \mathbf{u}(r,\varphi)$ one recognizes the anti-plane motion (u_z) to depend on ϕ_2 only and is decoupled from the other parts. This gives that equation (2.2) reduces to the 2D Helmholtz equation,

$$\Delta u_z + k_s^2 u_z = 0. \tag{2.10}$$

2.2 Green's Function Method

The Green's function method is a method for solving partial differential equations. This can be performed on many different sets of partial differential equations. The mathematical limitations and proofs are not addressed in this thesis. For the PDE, with its differential operator L, defined in

$$L(u)(\mathbf{x}) = f(\mathbf{x}), \quad u \text{ in } V, \tag{2.11}$$

the solutions is given by the integral

$$u(\mathbf{x}) = \int_V G(\mathbf{x};\mathbf{x}')f(\mathbf{x}')d\mathbf{x}', \tag{2.12}$$

where G is the Green's function. The Green's function is defined with its differential operator and the boundary conditions. Using GFM there are *only* two things which are complicated, finding the Green's function and evaluating the integral in equation (2.12). Finding the Green's function for a multi dimension problem is very complicated.

In this thesis eigenfunction expansion is used to simplify the derivation of a Green's function in a two dimensional problem to an one dimensional problem. The procedure to find the Green's function for a single dimension differential equation, ODE, is introduced. Deriving Green's functions for PDEs is described by Folland in *Fourier Analysis and its applications* [6].

2.2.1 Finding the Green's Function for a ODE

To find the Green's function it is important to both define the domain and the boundary conditions ($B(u)$). To keep the method somewhat general we consider the problem as

$$\begin{aligned}L(u)(x) = f(x), \quad x \in]a,b[, \quad a,b \text{ do not need to be finite,} \\ B(u) = 0.\end{aligned} \tag{2.13}$$

The boundary conditions are homogeneous in order to keep it as simple as possible. This is reasonable since a non homogeneous boundary condition can be transfered to the differential equation instead.

The Green's function is the function which solves the differential equation defined in

$$\begin{aligned} L(G)(x) &= \delta(x - x'), \quad x' \in]a,b[, \\ B(G) &= 0, \\ & L \text{ is a Sturm-Liouville operator, i.e.} \\ L(u) &= -(\partial_x p(x)\partial_x u) + (q(x) - \lambda w(x))u. \end{aligned} \tag{2.14}$$

The Green's function should be on the following form

$$G(x;x) = \begin{cases} c_1 u_0(x), & x < x', \\ c_2 u_1(x), & x > x'. \end{cases} \tag{2.15}$$

where each of the functions, u_0 and u_1 satisfies $L(u)(x) = 0$ and meets the boundary conditions for $x = a$ or b, respectively.

The Green's function is required to be continuous and its derivative discontinuous and equal to $p(x')$, defined in (2.14). Mathematically this is

$$\begin{aligned} & c_1 u_0(x') - c_2 u_1(x') = 0, \\ & c_1 u_0'(x') - c_2 u_1'(x') = -\frac{1}{p(x')}, \quad p(x) \text{ is from Sturm-Liouville operator,} \\ & \Rightarrow \begin{pmatrix} c_1 \\ c_2 \end{pmatrix} = \frac{1}{p(x')(u_0(x')u_1'(x') - u_0'(x')u_1(x))} \begin{pmatrix} -u_2(x') \\ -u_1(x') \end{pmatrix}. \end{aligned} \tag{2.16}$$

The determinant of the matrix is called the *Wronskian* and for a unique solution it must be nonzero. Using the results from equation (2.16) one can finalize the derivation of the Green's function

$$G(x;x') = \begin{cases} \frac{-u_0(x)u_1(x')}{Wp(x')}, & x < x' \\ \frac{-u_1(x)u_0(x')}{Wp(x')}, & x > x' \end{cases}, \quad W = u_0(x')u_1'(x') - u_1(x')u_0'(x'). \tag{2.17}$$

2.2.2 Free space Green's function

There are several different ways to derive the Green's function for free space. The boundary conditions are the radiation condition, i.e. no outgoing waves from infinity, as well as that the Green's function should be bounded at the origin. In this thesis the derivation is following the steps outlined earlier. First the boundary value problem for

$G(r,\varphi;r',\varphi')$ is

$$\begin{aligned}\Delta G(r,\varphi;r',\varphi') + k^2 G(r,\varphi;r',\varphi') &= -\frac{\delta(r-r')}{r}\delta(\varphi-\varphi'),\\ G(r,\varphi;r',\varphi') &= G(r,\varphi+2\pi;r',\varphi'),\\ G(r,\varphi;r',\varphi') &\quad \text{G remains finite as } r\to 0,\\ \lim_{r\to\infty}(\partial_r G(r,\varphi;r',\varphi') - ikG(r,\varphi;r',\varphi')) &= 0, \text{ radiation condition.}\end{aligned} \tag{2.18}$$

The φ dependence of the PDE is expanded as an exponential function series and this simplifies the problem further to

$$\begin{aligned}G(r,\varphi;r',\varphi') &= \sum_{m=-\infty}^{\infty} e^{im(\varphi-\varphi')} g_{m,f}(r;r'),\ \varphi\in[-\pi,\pi]\\ \Big(\frac{1}{r}\partial_r r\partial_r g_{f,m}(r;r') + (k^2 - \frac{m^2}{r^2})g_{m,f}(r;r')\Big)e^{im(\phi-\phi')} &= -\frac{\delta(r-r')}{r}\delta(\varphi-\varphi').\end{aligned} \tag{2.19}$$

It is now possible to utilize the orthogonality of the exponential function and reduce the PDE to a ODE. The ODE which is obtained is

$$\Big(\partial_r r\partial_r g_{f,m}(r;r') + (rk^2 - \frac{m^2}{r})g_{m,f}(r;r') = \delta(r-r'), \tag{2.20}$$

and the equation is recognized as the Bessel equation. The solutions to the Bessel equation are linear combinations of Bessel functions, $\mathrm{J}_m(x)$, and Neumann functions, $\mathrm{N}_m(x)$. Now the Green's function is defined as in equation (2.15)

$$g_{f,m}(kr) = \begin{cases} c_1 u_0(kr), & r<r',\\ c_2 u_1(kr), & r>r'.\end{cases} \tag{2.21}$$

Application of the boundary condition gives

$$\begin{aligned}u_0 \text{ remains finte as } r\to 0 \ &\Rightarrow u_0(kr) = \mathrm{J}_m(kr),\\ \lim_{r\to\infty}\partial_r u_1 - iku_1 = 0 &\Rightarrow u_1(kr) = \mathrm{J}_m(kr) + i\mathrm{N}_m(kr) \equiv \mathrm{H}_m^{(1)}(kr).\end{aligned} \tag{2.22}$$

Now the result from equation (2.17) is used and the final form of the free space Green's function is derived,

$$\begin{aligned}G(r,\varphi;r'\varphi') &= \frac{i}{4}\sum_{m=-\infty}^{\infty} e^{im(\varphi-\varphi')}\mathrm{J}_m(kr_<)\mathrm{H}_m^{(1)}(kr_>) \equiv\\ &\equiv \frac{i}{4}\begin{cases}\sum_{m=-\infty}^{\infty} e^{im(\varphi-\varphi')}\mathrm{J}_m(kr)\mathrm{H}_m^{(1)}(kr'), & r<r',\\ \sum_{m=-\infty}^{\infty} e^{im(\varphi-\varphi')}\mathrm{J}_m(kr')\mathrm{H}_m^{(1)}(kr), & r>r'.\end{cases}\end{aligned} \tag{2.23}$$

The simplification of the Wronskian is possible because of the recurrence formulas, cf. [2] p. 507.

For later applications the free space Green's function on integral form in rectangular coordinates is preferred. The free space Green's function is derived using a Fourier transform in rectangular coordinates, cf Boström [1],

$$G(x,y;x',y') = \frac{i}{4\pi}\int_{-\infty}^{\infty}\frac{1}{h}\exp(i(q(x-x_0)+h|y-y_0|))\mathrm{d}q, \quad h=\sqrt{k^2-q^2}. \tag{2.24}$$

2.2.3 Derivation of Green's function for cylindrical geometry

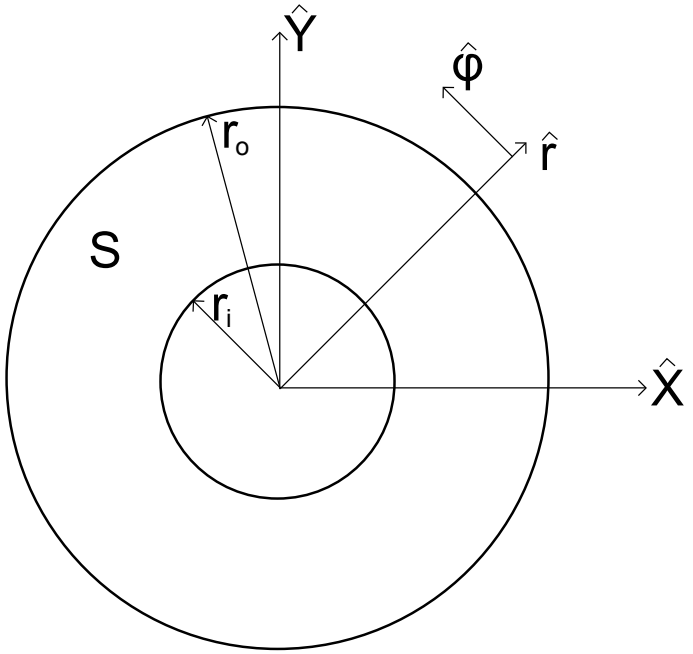

Figure 2.1: The figure shows the pipe for the problem in a polar geometry with the inner radius r_i and the outer radius r_o

The derivation of the Green's function for the cylindrical geometry, see figure 2.1, is a simple modification of the free space Green's function. The new domain for the pipe is

$$S := \{r \in [r_i,r_o], \quad \varphi \in [-\pi,\pi]\} \tag{2.25}$$

Since the domain is even the exponential function in the free space Green's function simplifies to a cosine function only. The new Green's function is two parts added to the

free space Green's function,

$$\begin{aligned} G(r,\varphi;r',\varphi') &= G_{Free} + G_{BC} = \sum_{m=0}^{\infty} (g_{m,free}(r;r') + g_{m,bc}(r,r')) \cos(m(\varphi-\varphi')), \\ g_{m,f}(r;r') &= \frac{i}{4}\varepsilon_m \mathrm{J}_m(kr_<)\mathrm{H}_m^{(1)}(kr_>), \\ g_{m,bc}(r;r') &= \mathrm{A}_m \mathrm{J}_m(kr) + \mathrm{B}_m \mathrm{N}_m(kr). \end{aligned} \tag{2.26}$$

The boundary conditions for the Green's function for the cylindrical geometry are homogeneous normal derivatives on both the inner and outer boundary. Due to the orthogonality of the trigonometric functions only the radial dependent parts are considered,

$$\begin{aligned} &\partial_r G(r_i,\varphi;r',\varphi') = \partial_r G(r_o,\varphi;r',\varphi') = 0 \Rightarrow \\ &\frac{i}{4}\varepsilon_m \mathrm{J}'_m(kr_i)\mathrm{H}_m^{(1)}(kr') + \mathrm{A}_m \mathrm{J}'_m(r_i) + \mathrm{B}_m \mathrm{N}'_m(r_i) = 0, \\ &\frac{i}{4}\varepsilon_m \mathrm{J}'_m(kr')\mathrm{H}_m^{(1)}(kr_o) + \mathrm{A}_m \mathrm{J}'_m(r_o) + \mathrm{B}_m \mathrm{N}'_m(r_o) = 0. \end{aligned} \tag{2.27}$$

The representation used for the Green's function does not involve A_m or B_m since the explicit dependence on r' is needed later on. The Green's function

$$\begin{aligned} G(r,\varphi;r',\varphi') = \sum_{m=0}^{\infty} \Big(&\alpha_m \mathrm{J}_m(kr_<)\mathrm{H}_m^{(1)}(kr_>) + \mathrm{A}_m^1 \mathrm{H}_m^{(1)}(kr')\mathrm{J}_m(kr) + \mathrm{A}_m^2 \mathrm{J}_m(kr')\mathrm{J}_m(kr) + \\ &+\mathrm{B}_m^1 \mathrm{J}_m(kr')\mathrm{N}_m(kr) + \mathrm{B}_m^2 \mathrm{H}_m^{(1)}(kr')\mathrm{N}_m(kr)\Big) \cos(m(\varphi-\varphi')), \end{aligned} \tag{2.28}$$

is obtained. Where the different terms are represented by:

$$\begin{aligned} \mathrm{A}_m^1 &= \frac{\alpha_m}{\gamma_m}\mathrm{N}'_m(kr_o)\mathrm{J}'_m(kr_i) \qquad \mathrm{A}_m^2 = -\frac{\alpha_m}{\gamma_m}\mathrm{N}'_m(kr_i)\mathrm{H}'^{(1)}_m(kr_o), \\ \mathrm{B}_m^1 &= \frac{\alpha_m}{\gamma_m}\mathrm{J}'_m(kr_i)\mathrm{H}'^{(1)}_m(kr_o) \qquad \mathrm{B}_m^2 = -\frac{\alpha_m}{\gamma_m}\mathrm{J}'_m(kr_o)\mathrm{J}'_m(kr_i), \\ \gamma_m &= \mathrm{J}'_m(kr_o)\mathrm{N}'_m(kr_i) - \mathrm{J}'_m(kr_i)\mathrm{N}'_m(kr_o), \\ \alpha_m &= \frac{i\varepsilon_m}{4}, \\ \varepsilon_m &= \begin{cases} 1, & m = 0, \\ 2, & m \neq 0. \end{cases} \end{aligned}$$

Now it is recognizable that the Green's function is divided into a singular (from the free space Green's function) and regular part (from the added parts).

2.3 The incident field

In this section the incident field is calculated using the eigenfunction expansion method. The calculations are very similar to the derivations of the free space Green's function.

The basic setup of the domain is a source situated at the outer edge symmetrically centered around φ_0. The source is, in radians, 2δ wide. The geometry is shown in figure 2.2. The mathematical formulation of the problem becomes,

$$\begin{aligned} \Delta u + k^2 u &= 0, \quad r \in [r_i, r_o], \quad \varphi \in [-\pi, \pi] \\ u(r,\varphi) &= u(r,\varphi + 2\pi), \\ \partial_r u(r_i,\varphi) &= 0, \\ \partial_r u(r_o,\varphi) &= F(\varphi), \\ F(\varphi) &= A\Theta(\varphi - (\varphi_0 - \delta))\Theta(\varphi_0 + \delta - \varphi). \end{aligned} \tag{2.29}$$

A is an arbitrary constant and Θ is the Heaviside step function Applying a separation of variables to the equation results in two ODEs instead of a PDE,

$$\Phi'' + \nu^2 \Phi = 0, \tag{2.30}$$

and

$$x^2 R''(x) + xR'(x) + R(x)(x^2 - \nu^2) = 0, \quad x = rk, \tag{2.31}$$

from the equation (2.30) $\nu^2 = m^2$ is obtained. Now it is possible to construct the solution as a sum of eigenfunctions,

$$u(r,\varphi) = \sum_0^\infty (A_m \sin(m\varphi) + B_m \cos(m\varphi))(C_m \mathrm{J}_m(kr) + D_m \mathrm{N}_m(kr)), \tag{2.32}$$

and by applying the boundary conditions at the inner radius,

$$\begin{aligned} \partial_r u(r_i,\varphi) = \sum_0^\infty (A_m \sin(m\varphi) + B_m \cos(m\varphi))k(C_m \mathrm{J}_m(kr_i) + D_m \mathrm{N}_m(kr_i)) = 0 \Rightarrow \\ C_m = -D_m \frac{\mathrm{N}'_m(kr_i)}{\mathrm{J}'_m(kr_i)}, \end{aligned} \tag{2.33}$$

is obtained. The boundary conditions on the outer radius is inhomogeneous thus more complicated,

$$\begin{aligned}
\partial_r u(r_o,\varphi) &= \sum_0^\infty (A'_m \sin(m\varphi) + B'_m \cos(m\varphi))k\left(\mathrm{N}'_m(kr_i) - \frac{\mathrm{J}'_m(kr_i)}{\mathrm{N}'_m(kr_o)}\mathrm{J}'_m(kr_i)\right) = F(\varphi),\\
A'_m &= \int_{-\pi}^{\pi} F(\varphi)\sin(m\varphi)\mathrm{d}\varphi = A\int_{\phi_o-\delta}^{\phi_0+\delta}\sin(m\varphi)\mathrm{d}\varphi, \quad m = 1,2,3...,\\
B'_m &= \int_{-\pi}^{\pi} F(\varphi)\cos(m\varphi)\mathrm{d}\varphi = A\int_{\phi_o-\delta}^{\phi_0+\delta}\cos(m\varphi)\mathrm{d}\varphi, \quad m = 1,2,3...,\\
B'_0 &= \int_{-\pi}^{\pi} F(\varphi)\mathrm{d}\varphi = A\int_{\phi_o-\delta}^{\phi_0+\delta}\mathrm{d}\varphi.
\end{aligned} \tag{2.34}$$

Collecting all the terms the solution of the incident field is obtained,

$$u(r,\varphi) = \sum_{m=0}^{\infty}\frac{2A\delta\sin(m\delta)}{m\delta}\frac{\cos(m(\varphi-\varphi_0))}{k(\mathrm{N}'_m(kr_o) - \frac{\mathrm{N}'_m(kr_i)}{\mathrm{J}'_m(kr_i)}\mathrm{J}'_m(kr_o))}(\mathrm{N}_m(kr) - \frac{\mathrm{N}'_m(kr_i)}{\mathrm{J}'_m(kr_i)}\mathrm{J}_m(kr)). \tag{2.35}$$

First GFM was tried for solving the problem since the Green's function for the domain is already derived. This was very tedious and computationally more difficult.

2.4 The scattered field

The solution of the scattered field can be achieved in several different ways; transfer matrix method, pure numerical methods and dual integral equations are some of the available methods. This thesis uses the hypersingular integral equation method which is a subset of the dual integral equation method. In this thesis the crack is placed along the x-axis, shown in figure 2.3, this is not a simplification since the source is placed at an arbitrary angle.

The scattered field is found using the integral representation,

$$u^{sc}(x,y) = \int_a^b \Delta u(x')\partial_{y'}(G(x,y;x',y'))\Big|_{y'=0}\mathrm{d}x', \tag{2.36}$$

where $\Delta u(x')$ is the crack opening displacement (COD). This is an application of a well known result from integral representation theory but is still shown and motived in 5.1. To solve for the COD a no stress condition is used on the crack,

$$\partial_y u^{sc}(x,y) + \partial_y u^{in}(x,y) = 0, \quad x \in [a,b], \quad y = 0. \tag{2.37}$$

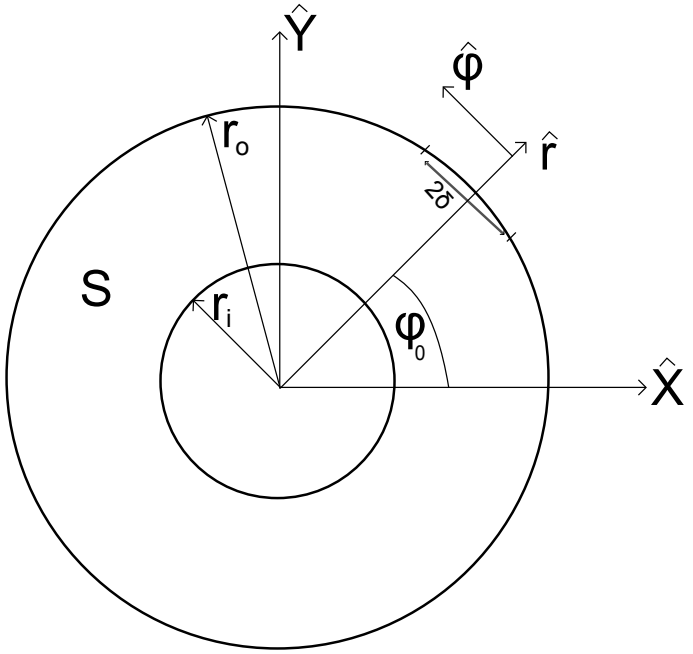

Figure 2.2: The figure shows the domain for the problem, the source is located symmetrically around φ_0. The width of the source is 2δ and it is located at the outer radius.

When applying $y = y' = 0$ inside the integral (2.36), the integral becomes singular and cannot be evaluated in a normal sense,

$$\begin{aligned}\lim_{y\to 0}\int_a^b \partial_y u^{sc}(x,y)\mathrm{d}x = -\lim_{y\to 0}\int_a^b \Delta u(x')\partial_y\partial_{y'}(G(x,y;x',y'))\Big|_{y'=0}\mathrm{d}x' \neq \\ \neq \int_a^b \Delta u(x')\partial_y\partial_{y'}(G(x,y;x',y'))\Big|_{y'=0,y=0}\mathrm{d}x'\end{aligned} \tag{2.38}$$

The reason for integral to become singular is the fact that the Green's function contains a Hankel function which for small arguments behaves as a logarithm,

$$\mathrm{H}_0^{(1)}(x) \to \log(x), \quad x \to 0. \tag{2.39}$$

When differentiating the logarithm twice a hypersingularity results, this is the reason for not taking both the limits inside the integral. This is regularized by projecting both

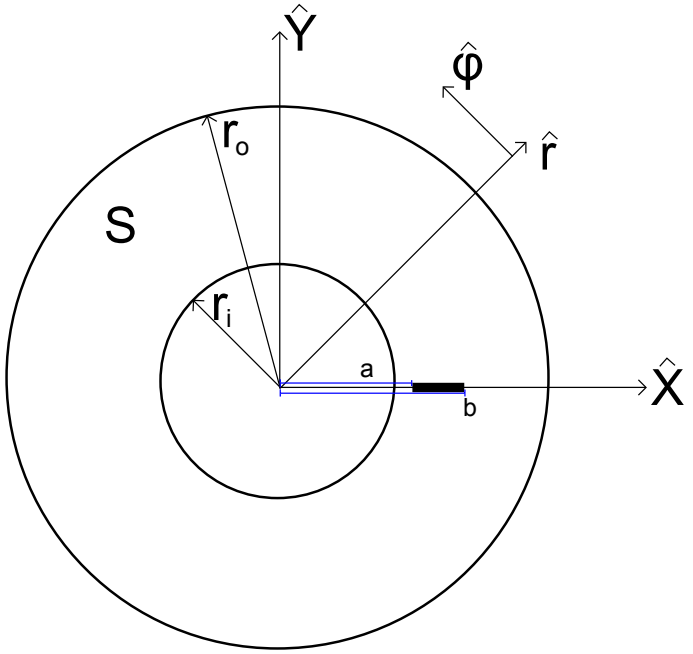

Figure 2.3: The figure shows the geometry and the location of the crack, as is seen it is placed in the radial direction along the x-axis. The crack begins at a and ends at point b.

the COD and equation (2.37) on Chebyshev functions, which have the correct square root beavior at the crack edges. In appendix 5.2 the Chebyshev functions are defined. The domain for the Chebyshev functions is minus $[-1,1]$, since the crack is not on this interval a linear transformation is used. The integral then becomes

$$\begin{aligned}
&\lim_{y\to 0}\int_a^b \overline{\psi}_n\left(\frac{2x-b-a}{b-a}\right)\partial_y u^{in}(x,y)\mathrm{d}x = -\lim_{y\to 0}\int_a^b \overline{\psi}_n\left(\frac{2x-b-a}{b-a}\right)\partial_y u^{sc}(x,y)\mathrm{d}x = \\
&= -\lim_{y\to 0}\int_a^b\int_a^b \overline{\psi}_n\left(\frac{2x-b-a}{b-a}\right)\Delta u(x')\partial_y\partial_{y'}(G(x,y;x',y'))\Big|_{y'=0}\mathrm{d}x'\mathrm{d}x = \\
&= -\int_a^b\int_a^b \overline{\psi}_n\left(\frac{2x-b-a}{b-a}\right)\Delta u(x')\partial_y\partial_{y'}(G(x,y;x',y'))\Big|_{y'=0,y=0}\mathrm{d}x'\mathrm{d}x.
\end{aligned} \tag{2.40}$$

The COD $\Delta u(x')$ is expanded in Chebyshev functions,

$$\Delta u(x') = \sum_{n'=1}^{N} \psi_{n'}(x')\alpha_{n'}, \tag{2.41}$$

inserting this into (2.40),

$$\lim_{y\to 0}\int_a^b \overline{\psi}_n\left(\frac{2x-b-a}{b-a}\right)\partial_y u^{in}(x,y)\mathrm{d}x = -\lim_{y\to 0}\int_a^b \overline{\psi}_n\left(\frac{2x-b-a}{b-a}\right)\partial_y u^{sc}(x,y)\mathrm{d}x =$$
$$= -\sum_{n'=1}^{N}\alpha_{n'}\int_a^b\int_a^b \overline{\psi}_n\left(\frac{2x-b-a}{b-a}\right)\psi_{n'}\left(\frac{2x'-b-a}{b-a}\right)\partial_y\partial_{y'}(G(x,y;x',y'))\Big|_{y'=0,y=0}\mathrm{d}x'\mathrm{d}x, \tag{2.42}$$

is obtained. To proceed it is necessary to split the Green's function into a regular (G_{BC}) and singular (G_{Free}) part,

$$G(x,y;x',y') = G_{Free}(x,y;x',y') + G_{BC}(x,y;x',y'),$$
$$G_{Free} = \frac{i}{4}\int_{-\infty}^{\infty}\frac{1}{h}\exp(i(q(x-x_0)+h|y-y_0|))\mathrm{d}q, \quad h=\sqrt{k^2-q^2},$$
$$G_{BC} = \mathrm{A}_m^1\mathrm{H}_m^{(1)}(kr')\mathrm{J}_m(kr) + \mathrm{A}_m^2\mathrm{J}_m(kr')\mathrm{J}_m(kr)+$$
$$+\mathrm{B}_m^1\mathrm{J}_m(kr')\mathrm{N}_m(kr)+\mathrm{B}_m^2\mathrm{H}_m^{(1)}(kr')\mathrm{N}_m(kr)\Big)\cos(m(\varphi-\varphi')). \tag{2.43}$$

the regular part will not be addressed more since it is easy to numerically integrate it. There is still work left with the singular part. A property of the Chebyshev function is

$$\int_{-1}^{1}\psi_n(s)e^{-i\gamma s}\mathrm{d}s = \frac{n}{\gamma}\mathrm{J}_n(\gamma), \tag{2.44}$$

applying this twice for the multiple integral containing the singular part the following is obtained,

$$\int_{-\infty}^{\infty}\int_a^b\int_a^b \overline{\psi}_n\left(\frac{2x-b-a}{b-a}\right)\psi_{n'}\left(\frac{2x'-b-a}{b-a}\right)\sqrt{k^2-q^2}e^{iq(x-x')}\mathrm{d}x\mathrm{d}x'\mathrm{d}q =$$
$$= nn'\int_{-\infty}^{\infty}\frac{\sqrt{k^2-q^2}}{q^2}\mathrm{J}_n(\frac{(b-a)q}{2})\mathrm{J}_{n'}(\frac{(b-a)q}{2})\mathrm{d}q. \tag{2.45}$$

The integral is convergent, however, the numerical computation is much faster if the range is reduced to a finite range, this is done by Van Den Berg [7]. Reducing the range changes the integral to

$$\frac{inn'}{4\pi}\int_{-\infty}^{\infty}\frac{\sqrt{k^2-q^2}}{q^2}\mathrm{J}_n(\tfrac{(b-a)q}{2})\mathrm{J}_{n'}(\tfrac{(b-a)q}{2})\mathrm{dq}=$$

$$=\begin{cases}\frac{nn'}{2\pi}\int_0^k\frac{\sqrt{k^2-q^2}}{q^2}\Big(\mathrm{J}_>(\tfrac{(b-a)q}{2})\mathrm{H}^{(1)}_<(\tfrac{(b-a)q}{2})+\frac{i\delta_{nn'}}{n\pi}\Big)\mathrm{dq}-\frac{n\delta_{nn'}}{4\pi}, & n+n' \quad \text{even}\\ 0, & n+n' \quad \text{odd},\end{cases} \tag{2.46}$$

$>$ is $\max(n,n')$, $<$ is $\min(n,n')$.

Collecting the different terms into an equation system,

$$-\int_a^b\overline{\psi}_n\left(\frac{2r-b-a}{b-a}\right)u^{in}(r,0)\frac{\mathrm{d}r}{r}=\alpha_{n'}Q_{n'n}. \tag{2.47}$$

α_n is the unknown coefficients of the COD, and $Q_{n'n}$ is

$$\begin{aligned}Q_{n'n}=\sum_m^{\infty}m^2\Big(&\mathrm{A}^1_m\int_a^b\psi_{n'}\left(\frac{2r'-b-a}{b-a}\right)\mathrm{H}^{(1)}_m(kr')\frac{\mathrm{d}r'}{r'}\int_a^b\overline{\psi}_n\left(\frac{2r-b-a}{b-a}\right)\mathrm{J}_m(kr)\frac{\mathrm{d}r}{r}+\\
&+\mathrm{A}^2_m\int_a^b\psi_{n'}\left(\frac{2r'-b-a}{b-a}\right)\mathrm{J}_m(kr')\frac{\mathrm{d}r'}{r'}\int_a^b\overline{\psi}_n\left(\frac{2r-b-a}{b-a}\right)\mathrm{J}_m(kr)\frac{\mathrm{d}r}{r}+\\
&+\mathrm{B}^1_m\int_a^b\psi_{n'}\left(\frac{2r-b-a}{b-a}\right)\mathrm{J}_m(kr')\frac{\mathrm{d}r'}{r'}\int_a^b\overline{\psi}_n\left(\frac{2r-b-a}{b-a}\right)\mathrm{N}_m(kr)\frac{\mathrm{d}r}{r}+\\
&+\mathrm{B}^2_m\int_a^b\psi_{n'}\left(\frac{2r'-b-a}{b-a}\right)\mathrm{H}^{(1)}_m(kr')\frac{\mathrm{d}r'}{r'}\int_a^b\overline{\psi}_n\left(\frac{2r-b-a}{b-a}\right)\mathrm{N}_m(kr)\frac{\mathrm{d}r}{r}\Big)+\\
&+\begin{cases}\frac{inn'}{2\pi}\int_0^k\frac{\sqrt{k^2-q^2}}{q^2}\Big(\mathrm{J}_>(\tfrac{(b-a)q}{2})\mathrm{H}^{(1)}_<(\tfrac{(b-a)q}{2})+\frac{i\delta_{nn'}}{n\pi}\Big)\mathrm{dq}-\frac{n\delta_{nn'}}{4\pi}, & n+n' \quad \text{even}\\ 0, & n+n' \quad \text{odd}.\end{cases}\end{aligned} \tag{2.48}$$

It is now possible to determine $\Delta u(x')$ and therefore determine the scattered field using equation (2.36) by evaluating the integral using a Gauss-Legendre quadrature.

3

Results

This chapter contains the results for both the incident field and the scattered field. The figures shows the real part of the field because it shows the wave fronts. The source term is centered around the the y-axis, thus $\varphi_0 = 90°$ and is $2\delta = 15°$ wide.

3.1 The incident field

The incident fields are calculated with no crack present and the results confirm strong influence on the frequency. Frequency is a very important parameter, however, it is more convenient to study the dimensionless parameter $k(r_o - r_i)$. The dimensionless number correlates to the number of wave fronts inside the pipe. There is an other dimensionless number which is important and it is ration between the inner and the outer radius. It is kept constant to 10 and why is discussed in detail in the discussion.

To verify the solution other parameters were varied, in figures 3.1(a) and 3.1(b) the frequency dependence is shown and in figures 3.1(c) and 3.1(d) dependence of the δ and φ_0 is shown.

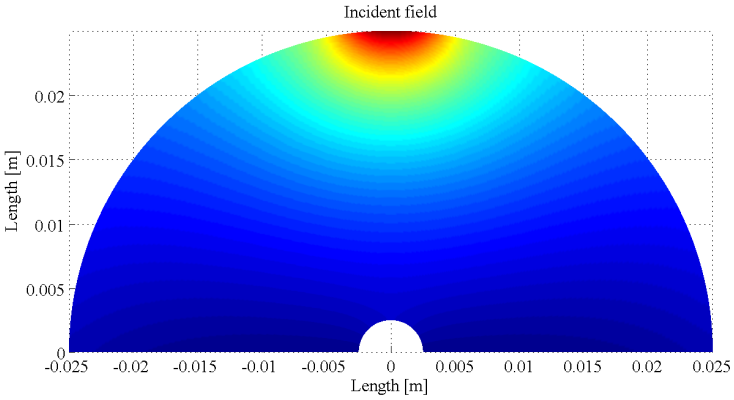

(a) The figure shows the incident field for a frequency where $k(r_o - r_i) = 1.78$.

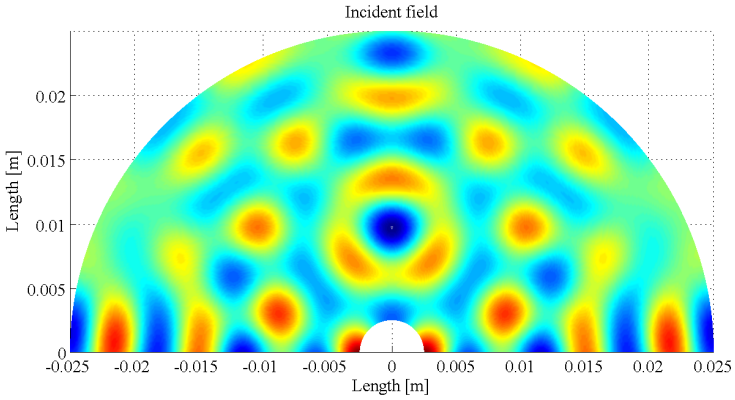

(b) The figure shows the incident field for a frequency where $k(r_o - r_i) = 22.2$.

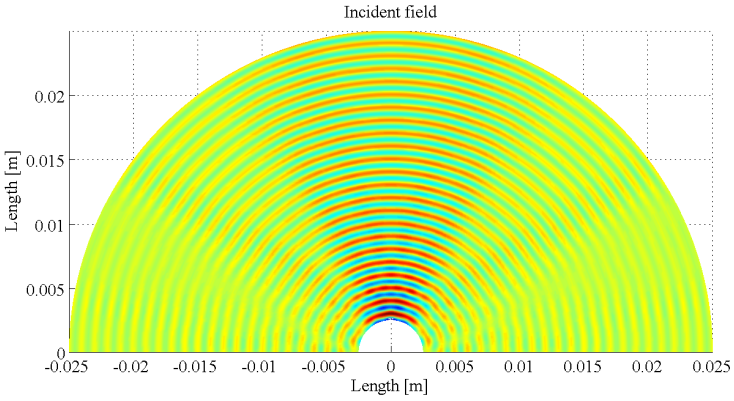

(c) The figure shows the incident field where the source is spans over $\frac{\pi}{3}$ (2δ)radians and φ_0 is centered around the y-axis, i.e. $\varphi_0 = \frac{\pi}{2}$.

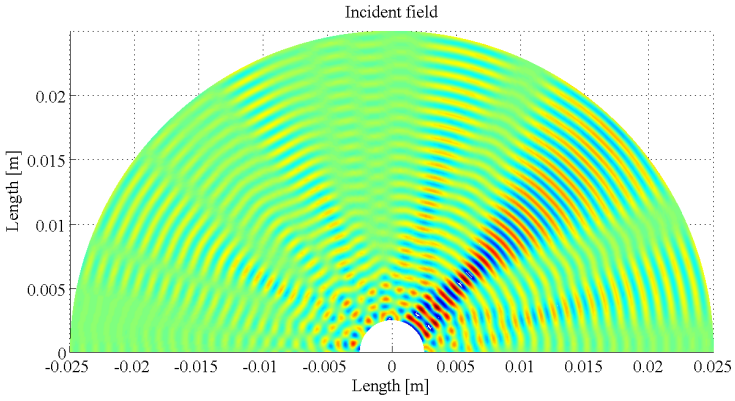

(d) The figure shows the incident field where the source is spans over $\frac{\pi}{12}$ (2δ) radians and φ_0 is centered at the angle $\frac{\pi}{4}$, which is along the line $y = x$.

Figure 3.1: The figure shows the evaluation of the incident field by varying the different parameters in the solution. In figures (a) and (b) only the frequency is changed, in figures (c) and (d) the frequency is kept the same, whilst varying the width and location of the source.

3.2 The scattered field

The results for the scattered fields are also compared between different dimensionless numbers $k(b-a)$ where $b-a$ is the length of the crack. This is a very similar comparison as for the incident field, but normalized with the length of the crack instead of the thickness of the pipe. The dimensionless number is referred to as the ka number, since a is a notation often used in the literature for the length of the crack. The crack length is a quarter of the wall thickness of the pipe.

The results are shown as a comparison between the incident and the scattered fields, the main comparison is between the total field (scattered field added to incident field). The scattered field is also divided into a regular part and a singular part and it shows that the regular part becomes larger when the wave number rises. The figures are ordered with the smallest wavenumber first and largest last.

The incident fields are created with the parameters selected earlier, $\delta = \frac{\pi}{24}$ and $\varphi_0 = \frac{\pi}{2}$.

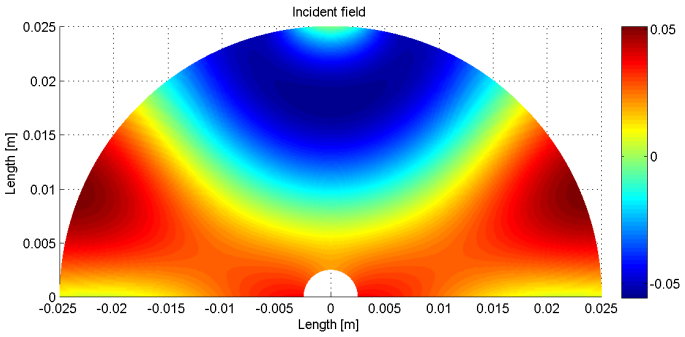

(a) The figure shows the incident field.

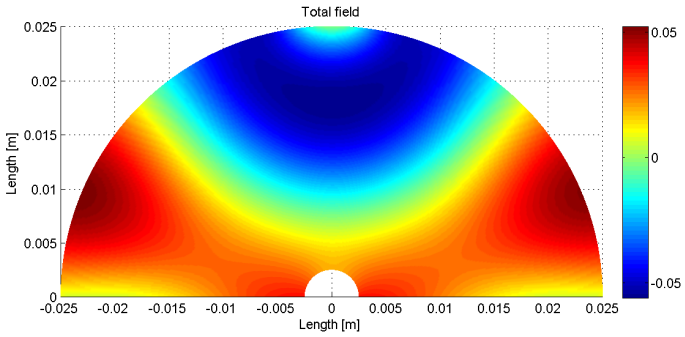

(b) The figure shows the real part of the total field.

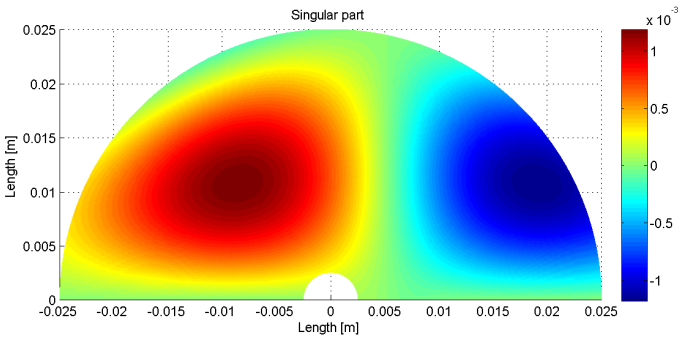

(c) The figure shows the scattered field which originates from the singular part of the hypersingular integral.

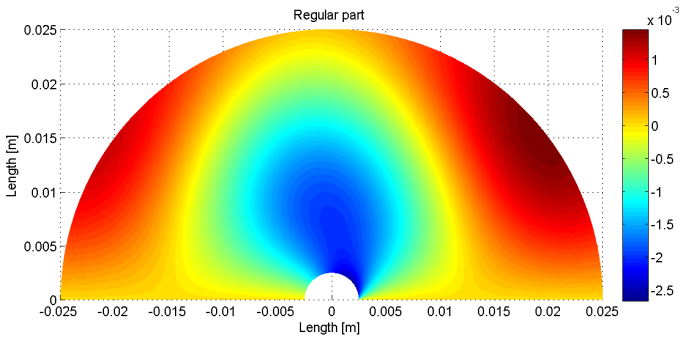

(d) The figure shows the scattered field which originates from the regular part of the hypersingular integral.

Figure 3.2: The figures shows the incident field (a), the total field (b), the part originating from the singular integral of the scattered field (c) and the part originating from the regular integral of the scattered field (d) for $ka \approx 1$.

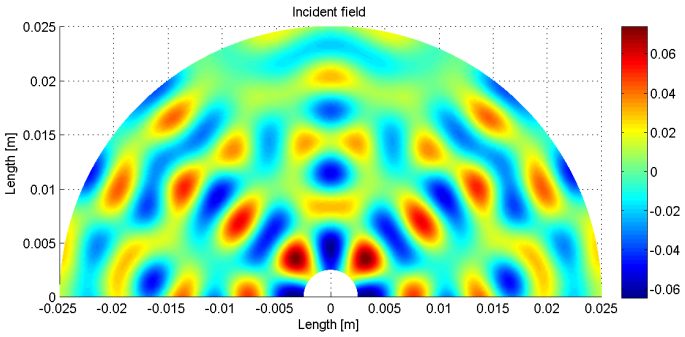

(a) The figure shows the incident field.

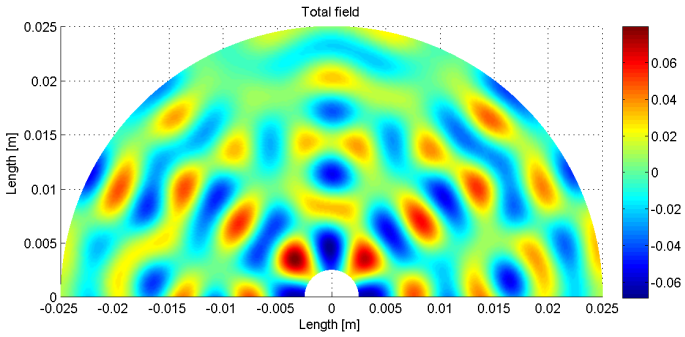

(b) The figure shows the real part of the total field.

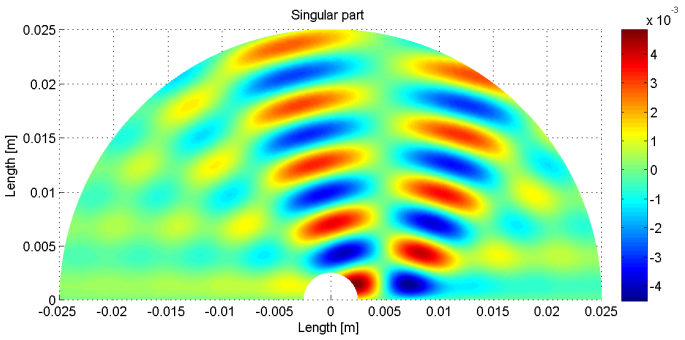

(c) The figure shows the scattered field which originates from the singular part of the hypersingular integral.

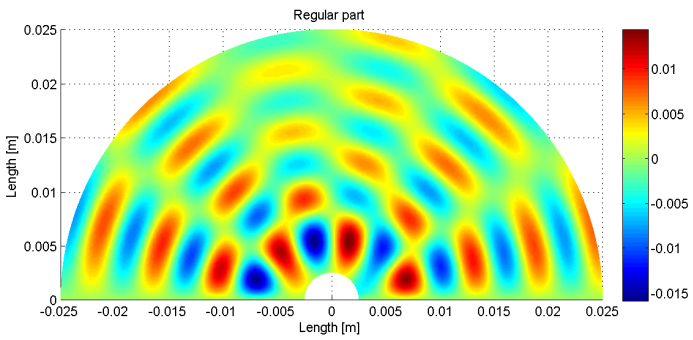

(d) The figure shows the scattered field which originates from the regular part of the hypersingular integral.

Figure 3.3: The figures shows the incident field (a), the total field (b), the part originating from the singular integral of the scattered field (c) and the part originating from the regular integral of the scattered field (d) for $ka \approx 6$.

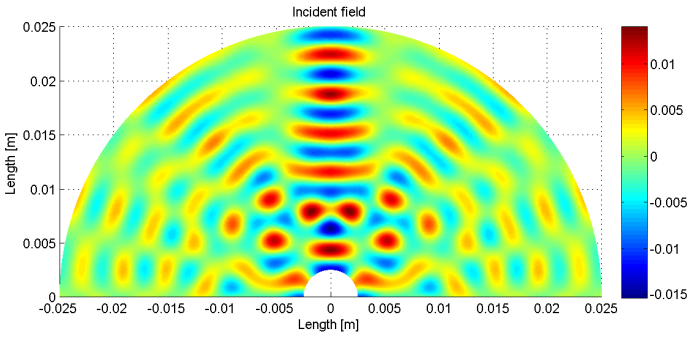

(a) The figure shows the incident field.

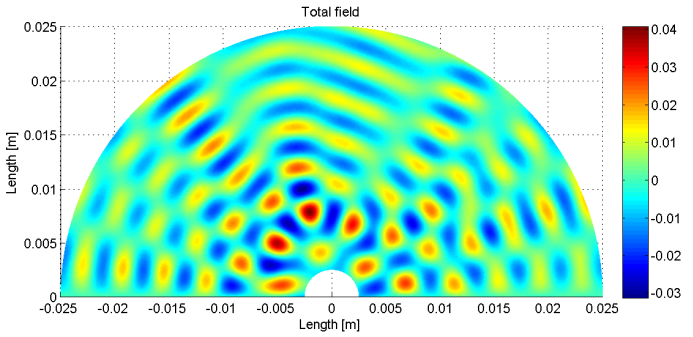

(b) The figure shows the real part of the total field.

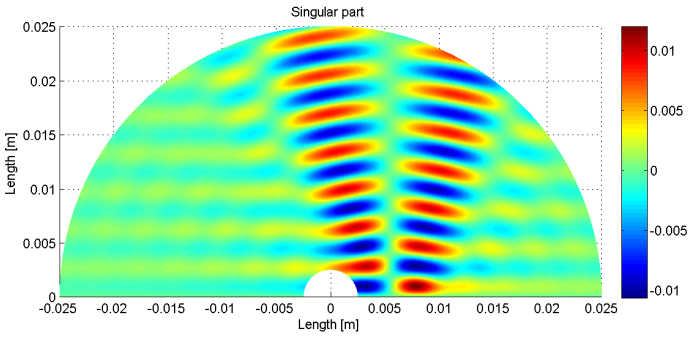

(c) The figure shows the scattered field which originates from the singular part of the hypersingular integral.

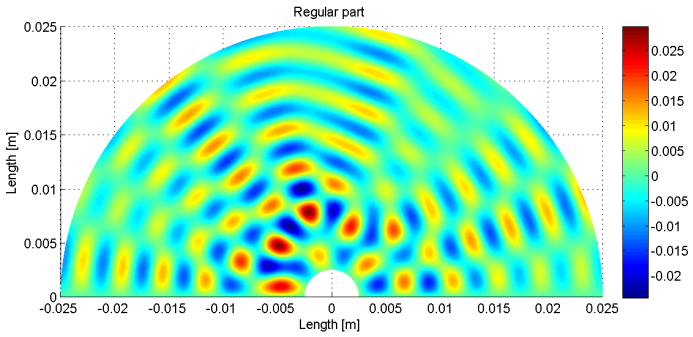

(d) The figure shows the scattered field which originates from the regular part of the hypersingular integral.

Figure 3.4: The figures shows the incident field (a), the total field (b), the part originating from the singular integral of the scattered field (c) and the part originating from the regular integral of the scattered field (d) for $ka \approx 10$.

4

Discussion

This chapter contains the discussion of the results and its merit. This includes a discussion about the numerical evaluation of the integrals as well as the fields. A brief discussion about what can be improved and how the changes can be implemented. The first item to be discussed is the choice of the size of the pipe, this choice has a big influence on the solution of the scattered fields obviously.

4.1 The pipe geometry

The ratio of the outer and inner radius in this thesis is much bigger than the pipes encountered in real life. This is because of the non stress condition of the crack, i.e. a incident field and the crack must interact. The incident field is propagating in the radial direction which focuses the main part of the wave on the center cavity instead of directly on the crack. The large ratio is to ensure parts of the incident field scatters on the crack. The incident field can be directed using methods derived by Boström and Wirdelius [8], this is an important step in order to model the scattered fields in pipes with different more realistic sizes.

4.2 Incident field

The incident field is, for this case, quite simple since it is an eigenfunction expansion in a known set of coordinates, where the eigenfunctions forms a base and are defined explicitly.

The numerics on this is very straightforward since there is only one part which needs to be truncated, the number of terms used in the series expansion. This number is truncated to 30, this number is constructed by trial and error, at an early stage several different truncations are used to find a suitable truncation. The same truncation is used

for the number of terms used in the series expansion in the scattered field. The boundary condition is imposed on the derivative, this makes the number of terms in the series expansion lower.

4.3 Scattered field

In this thesis the comparison between the singular and regular part of the integral is performed and it is obvious that from the singular part the crack reflects in a manner similar to what is expected. The regular part seems to give a scattering pattern which is not as localized as the singular part, which also is expected.

The scattered field, unlike the incident field, needs the evaluation of several integrals numerically. The integrals are evaluated using a Gauss-Legendre quadrature. There are several different integrals over several different ranges, all of them are tested widely. The largest range evaluated using numerical methods is the infinite range in particular when evaluating the scattered field, singular part of the Greens function in (2.36). The truncation is done w.r.t the factor k. The convergence test of the integral is shown in table 4.1

Table 4.1: The convergence of the integral in equation (2.36). The range of the integral is truncated w.r.t. k since the k dependence forces the integral to be convergent for large k. The integral is also, for this comparison truncated to half the interval, only for the convergence test not when evaluating the scattered field.

Range	number of Gauss points	Norm(field)
0-2k	200	$3.286 \cdot 10^{-9}$
0-2k	300	$3.286 \cdot 10^{-9}$
0-2k	1000	$3.286 \cdot 10^{-9}$
0-5k	500	$3.284 \cdot 10^{-9}$
0-10k	1000	$3.286 \cdot 10^{-9}$
0-10k	2000	$3.285 \cdot 10^{-9}$
0-10k	500	$3.287 \cdot 10^{-9}$
0-100k	500	$3.374 \cdot 10^{-9}$
0-100k	2000	$3.286 \cdot 10^{-9}$

From table 4.1 the range of the integral, equation (2.36), is truncated to $-10k$ to $10k$ and 2000 Gauss-Legendre points are used. The table shows that a smaller range and fewer integration points can be used, however the time gain was not enough to motivate this.

4.4 Future work

The time complexity of this problem is in the order of `N·m·nR·nPhi`, where `N` is the truncation of the series expansion of the COD, `m` is the number of terms in the series expansion of the incident field, `nR` is the number of mesh points in the radial direction and `nPhi` is the number of mesh points in the angular direction. The number used for these are; `N` = 8, `m` = 30, `nR` = 200 and `nPhi` = 400. This means that for solving for the scattered field all integrals and coefficients need to be evaluated approximately 19 million times. To enhance the speed it is beneficial to program in a language for high speed computation instead of Matlab, e.g. Python or Fortran.

There are many terms that occur at many places, it can be beneficial to calculate them once and store them in a list and loading the values form the list instead of re-evaluating them every time, e.g. A_m^1, A_m^2, B_m^1 and B_m^2.

This thesis is a small part of modeling a 3D pipe. This model can be helpful for completing this task. This thesis is a good way to introduce the method for crack scattering problems. Later on the results in the thesis can be used for comparison with results from the full 3D model.

5

Appendix

5.1 Integral representation for scattered flow

The integral representation for the scattered field is derived by multiplying the equation of motion with the Green's function,

$$G(\mathbf{r};\mathbf{r}')\nabla^2 u(\mathbf{r}) + G(\mathbf{r};\mathbf{r}')k^2 u(\mathbf{r}) = 0, \tag{5.1}$$

and the Green's functions differential equation multiplied by the displacement,

$$u(\mathbf{r})\nabla^2 G(\mathbf{r};\mathbf{r}') + u(\mathbf{r})k^2 G(\mathbf{r};\mathbf{r}') = u\delta(\mathbf{r}-\mathbf{r}'). \tag{5.2}$$

Subtracting the first equation with the second and using a vector identity

$$\nabla\cdot(u(\mathbf{r})\nabla G(\mathbf{r};\mathbf{r}') - G(\mathbf{r};\mathbf{r}')\nabla u(\mathbf{r})) = u(\mathbf{r})\delta(\mathbf{r}-\mathbf{r}'), \tag{5.3}$$

is obtained. Integration over the volume, figure 5.1, yields

$$\int_S (u(\mathbf{r})\nabla G(\mathbf{r};\mathbf{r}') - G(\mathbf{r};\mathbf{r}')\nabla u(\mathbf{r}))\cdot \mathbf{n}\mathrm{d}S' = \begin{cases} u(\mathbf{r}), & \mathbf{r}' \text{ in volume} \\ 0, & \text{otherwise.} \end{cases} \tag{5.4}$$

Using that both u and G satisfies the boundary condition, i.e. along S_1 the normal derivative for both of them is zero, the following is obtained

$$u - \int_{S^{in}} (u\nabla G - G\nabla u)\cdot \mathbf{n}\mathrm{dS} \equiv u - u^{in} = \int_{S^{sc}} (u\nabla G - G\nabla u)\cdot \mathbf{n}\mathrm{dS} = \int_{S^{sc}} u\nabla G\cdot \mathbf{n}\mathrm{dS} \equiv u^{sc}.$$

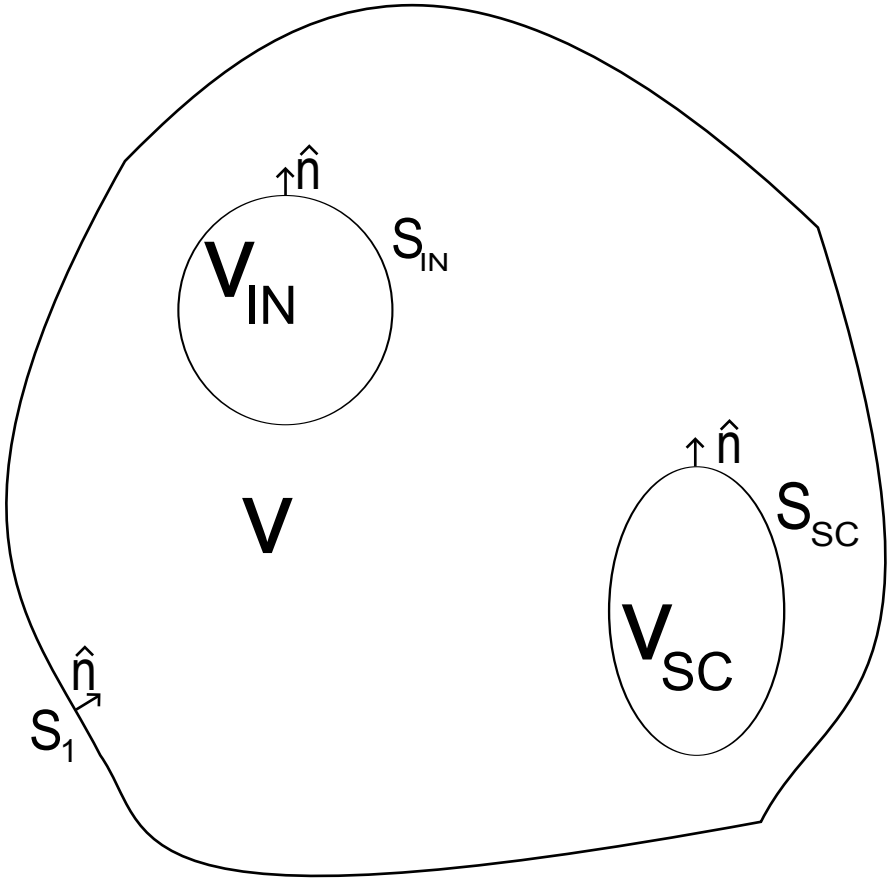

Figure 5.1: The figure shows a generic volume with a source, V_{in}, and a volume which reflects the incoming wave, V_{sc} as well as their surfaces and normal derivatives.

5.2 Chebyshev functions

The Chebyshev functions are defined as

$$\psi_n(s) = \begin{cases} \frac{1}{\pi}\cos(n\arcsin(s)) & n = 1,3,... \\ \frac{i}{\pi}\sin(n\arcsin(s)) & n = 2,4,... \end{cases} \tag{5.5}$$

and they are an orthogonal base [1].The functions are of the form $\sqrt{1-s^2}$ and it is the property at $s \pm 1$ that corresponds to the singularity at the edge of the crack which regulates the hypersingular integral. Another important property is

$$\int_{-1}^{1} \psi_n(s) e^{-i\gamma s} \mathrm{ds} = \frac{n}{\gamma} \mathrm{J}_n(\gamma). \tag{5.6}$$

Bibliography

[1] A. Boström, *Review of hypersingular integral equation method for crack scattering and application to modeling of ultrasonic nondestructive evaluation*, Applied Mechanics Reviews 56 (4) (2003) 383–405.
URL http://link.aip.org/link/?AMR/56/383/1

[2] G. Arfken, *Mathematical Methods for Physicists*, Academic Press, London, 1970.

[3] P. A. Martin, F. J. Rizzo, *Hypersingular integrals: how smooth must the density be?*, Int. J. Numer. Methods Eng. 39 (1996) 687–704.
URL http://onlinelibrary.wiley.com/doi/10.1002/%28SICI%291097-0207%2819960229%2939:4%3C687::AID-NME876%3E3.0.CO;2-S/abstract

[4] A. Boström, *Fundamental Structural Dynamics*, 2001.

[5] K. F. Graff, *Wave Motion in Elastic Solids*, Dover Publications, 1991.

[6] G. B. Folland, *Fourier analysis and its applications*, The Wadsworth & Brooks/Cole mathematics series, Brooks Cole, 1992.

[7] P. M. van den Berg, *Transition matrix in acoustic scattering by a strip*, Journal of the Acoustical Society of America 70 (1981) 615–619.
URL http://adsabs.harvard.edu/abs/1981ASAJ...70..615V

[8] A. Boström, H. Wirdelius, *Ultrasonic probe modeling and nondestructive crack detection*, Journal of the Acoustical Society of America 97 (5) (1995) 2836–2848.
URL http://asadl.org/jasa/resource/1/jasman/v97/i5/p2836_s1